Progress In Electromagnetics Research, Vol. 174, 43–53, 2022

Comparison of Correlation Performance for Various Measurement Schemes in Quantum Bipartite Radar and Communication Systems

Rory A. Bowell[1], Matthew J. Brandsema[1], Ram M. Narayanan[1, *], Stephen W. Howell[2], and Jonathan M. Dilger[2]

Abstract—Bipartite systems have become popular in emerging quantum radar and quantum communication systems. This paper analyzes the various correlation coefficients for different types of quantum radar measurement schemes, such as: (i) immediate detection of the idler photon events to be used in post-processing correlation with the signal photon events, (ii) immediate detection of the idler electric field to be used in post-processing correlation with the signal electric field, (iii) immediate detection of the idler quadratures to be used in post-processing correlation with the signal quadratures, and (iv) conventional analog correlation method of the optical parametric amplifier. The showcased results compare the performance of these different methodologies for various environmental scenarios. This work is important at developing the fundamentals behind quantum technologies that require covariance measurements and will permit more accurate selection of the appropriate measurement styles for individual systems.

1. INTRODUCTION

Classical technologies have been used for decades in the radar and communication applications. While it is understood that classical radar and communication are functional, we are approaching the limits to which they can be improved. As technology improvements bring us close to these limits, it is necessary to utilize new approaches to stop counter technologies from deeming it irrelevant.

Quantum systems have been shown to enhance the performance of both radar and communication by improving the ability to discern weak received signals from the noise or providing a secure propagation channel [1–8]. While there are many useful properties intrinsic to quantum mechanics, the main ability to assist with this performance improvement is through quantum entanglement [9].

A quantum radar system works through the creation of entangled signal and idler photons through spontaneous parametric down conversion (SPDC) [10]. The creation of these photons at the same time allows for a perfect temporal correlation allowing for easier discernment from noise photons. With this easier discrimination caused by synchronous creation, bipartite entanglement has been shown to have a 3-dB improvement in the error exponential [1, 11–15]. Bipartite quantum radar has been a topic of discussion in research [16, 17], but a direct comparison between the photon counting measurements and the electric field measurement has not been evaluated. This paper seeks to explain the theoretical basis of current research. Namely, using quadrature measurements while also counting photons and correlating them later. We seek to compare the correlation performance of these new techniques. A general setup for one of these systems is seen in Figure 1.

More specifically, there has been recent work showcasing a quantum advantage using classical measurements of electric field quadratures [16, 18] and by immediately detecting the idler photon counts

Received 25 February 2022, Accepted 11 May 2022, Scheduled 23 May 2022

* Corresponding author: Ram M. Narayanan (ram@engr.psu.edu).

[1] Department of Electrical and Computer Engineering, The Pennsylvania State University, University Park, PA 16802, USA. [2] Naval Surface Warfare Center, Crane Division, 300 Highway 361, Crane, IN 47522, USA.

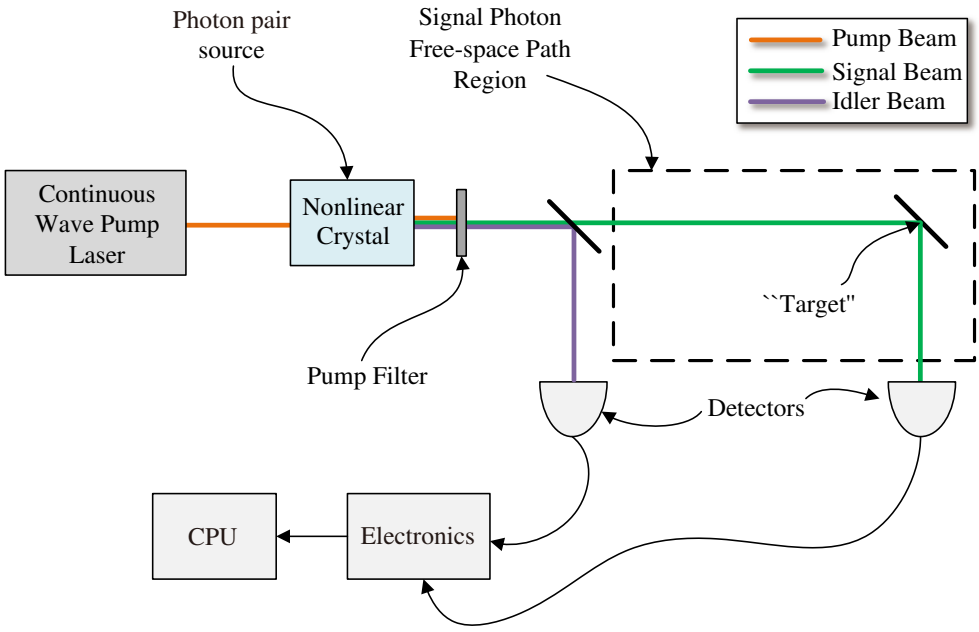

Figure 1. The general experimental setup for the measurement schemes discussed. In all cases, the idler photon is measured immediately and correlated with the returning signal photon at a later point in time. The detectors can vary between single photon counters and electric field sensors.

and correlating later with the signal counts [19]. These methodologies are very similar to classical noise radar techniques done in the past [15]. The goal of this paper is to analyze the correlation performance of these type of systems and determine which method performs the best for a given situation.

It is important to note that the calculations performed in this paper represent overall correlations from large data sets consisting of separate and time-separated measurements of the signal and idler streams. Indeed, electric field measurements necessarily involve many photon measurements due to the inability to simultaneously measure the photon number and electric field with arbitrary precision because of the operators not being commutable.

Here, we mathematically evaluate a two-mode squeezed vacuum acted on by the number operator (photon counting), the electric field operator (electric field measurement), and the electric field quadrature [20]. In our evaluation, we solve for all parts of the covariance matrix and determine the covariance between the signal and idler beams for each system [18, 21]. Additionally, we show a comparison between the photon counting and electric field temporal covariance.

This paper is structured as follows. Section 2 develops the mathematics associated with the electric field covariance. In Section 3, we develop the theory leading to the number operator covariance and compare the results with the electric field covariance. Section 4 analytically formulates the electric field quadrature covariance. In Section 5 a detailed analysis is presented of all three covariance results for different operational scenarios. Conclusions are presented in Section 6.

2. ELECTRIC FIELD COVARIANCE

The electric field operator refers to the bulk measurement of the electric fields of the signal and idler streams of photons. The correlation between the signal and immediately detected idler would be found using a digitizer.

We begin with the electric field operator defined by [22]:

$$E(r,t) = \sum_k \hat{\epsilon}_k \mathcal{E}_k a_k e^{-i\chi} + \hat{\epsilon}_k \mathcal{E}_k a_k^\dagger e^{i\chi} \tag{1}$$

where $\hat{a}_k$ is the creation operator for the frequency mode, k, and χ is the phase (which we can suppress

by assuming that the signal and idler are aligned in time and space via post processing), $\hat{\epsilon}_k$ is a unit polarization vector, and

$$\mathcal{E}_k = \left(\frac{\hbar\nu_k}{2\epsilon_0 V}\right)^{\frac{1}{2}} \tag{2}$$

where $\hbar$ is the Planck's constant divided by 2π; ν_k is the frequency associated with the momentum mode k; ϵ_0 is the permittivity of free space; and V is the quantization volume. $\mathcal{E}_k$ will be suppressed since it will be canceled in the final correlation calculations due to the fact these correlations are normalized. This will allow for greater calculation simplicity and easier to understand solutions. The integral formalism is also not required for the solution as we assume the field is approximately monochromatic (a single momentum mode) where future work will look at a full band signal. For an aligned signal and idler measurement with a linear polarization, Equation (1) reduces to:

$$\hat{E} = \hat{a} + \hat{a}^\dagger \tag{3}$$

We now begin with with a two-mode squeezed state:

$$|\psi\rangle = \gamma \sum_{n=0}^{\infty} \beta^n |n,n\rangle_{i,s} \tag{4}$$

where i and s stand for *idler* and *signal* respectively, $\gamma = \sqrt{\frac{1}{N_s+1}}$, $\beta = \sqrt{\frac{N_s}{N_s+1}}$, and N_s is the mean photon number per mode. This state is entangled and is the output of a continuous-wave pumped spontaneous parametric down-conversion (SPDC) source.

To find the covariance between the signal and idler, we need to derive the electric field covariance matrix. It should be noted that the physically realizable version of this state is a tensor product between Equation (4) and the thermal noise state. Formally, this calculation is done with a density matrix approach, as a density matrix fully describes a physical system's quantum state, including its statistical mixture with surrounding systems by including all possible projectors the system can collapse into, and their associated probabilities [23, 24]. We first define the density matrix for the two-mode squeezed vacuum state:

$$\rho_{\text{TMSV}} = \frac{1}{N_s+1} \sum_{m=0}^{\infty}\sum_{n=0}^{\infty} \left(\frac{N_s}{N_s+1}\right)^{\frac{n+m}{2}} |n,n\rangle\langle m,m| \tag{5}$$

and the density matrix for the noise state [23]:

$$\rho_T = \frac{1}{N_T+1} \sum_{i=0}^{\infty} \left(\frac{N_T}{N_T+1}\right)^{i} |i\rangle\langle i| \tag{6}$$

where $N_T = \frac{1}{1-\kappa} N_B$ and N_B is the mean photon number per mode in the noise path [11]. The return density matrix will be a tensor product between these two matrices:

$$\begin{aligned} \rho_{\text{return}} &= \rho_{\text{TMSV}} \otimes \rho_T \\ &= \frac{1}{N_T+1}\frac{1}{N_s+1} \sum_{n=0}^{\infty}\sum_{m=0}^{\infty}\sum_{i=0}^{\infty} \left(\frac{N_s}{N_s+1}\right)^{\frac{n+m}{2}} \\ &\quad \times \left(\frac{N_T}{N_T+1}\right)^{i} |n,n,i\rangle\langle m,m,i| \end{aligned} \tag{7}$$

This can be used to find the expectation value of an arbitrary operator, $\hat{O}$, by taking the trace of this density matrix with the operator applied to it.

$$\langle\hat{O}\rangle = \text{tr}(\rho_{\text{return}}\hat{O}) \tag{8}$$

$$\begin{aligned} &= \langle m,m,j| \frac{1}{N_T+1}\frac{1}{N_s+1} \sum_{n=0}^{\infty}\sum_{m=0}^{\infty}\sum_{i=0}^{\infty} \left(\frac{N_s}{N_s+1}\right)^{\frac{n+m}{2}} \\ &\quad \times \left(\frac{N_T}{N_T+1}\right)^{i} |n,n,i\rangle\langle m,m,i|\hat{O}|m,m,j\rangle \end{aligned} \tag{9}$$

This formalism is only required when dealing with modes that include appreciable thermal noise contributions, $\hat{a}_B$, due to the complete separation of the ensembles between the noise and signal/idler modes. Therefore, for situations which have insignificant thermal background noise contributions, such as quantities involving the stored idler stream in the transceiver, we perform equivalent, but simpler in operation, state calculations.

Having determined the approach for performing the calculations, simplifications will be introduced. First, the quantum covariance is defined as [25]:

$$\mathrm{Cov}\left(\hat{A},\hat{B}\right) = \frac{1}{2}\left(\left\langle\left\{\hat{A},\hat{B}\right\}\right\rangle - \langle\hat{A}\rangle\langle\hat{B}\rangle\right) \tag{10}$$

For monochromatic fields, since the electric field operators between modes are commutative, i.e.:

$$[\hat{E}_1,\hat{E}_2] = \hat{E}_1\hat{E}_2 - \hat{E}_2\hat{E}_1 = 0 \tag{11}$$

this allows us to set $\langle\hat{E}_1\hat{E}_2\rangle = \langle\hat{E}_2\hat{E}_1\rangle$, thereby simplifying future calculations. It also allows the quantum covariance shown in Equation (10) to be equivalent to the classical covariance $\langle AB\rangle - \langle A\rangle\langle B\rangle$. The state shown in Equation (4) is a zero mean Gaussian state; therefore the covariance reduces to $\langle AB\rangle$. Consequently, we find the covariance matrix to be:

$$V = \begin{pmatrix} \langle\hat{E}_s^2\rangle & \langle\hat{E}_s\hat{E}_i\rangle \\ \langle\hat{E}_i\hat{E}_s\rangle & \langle\hat{E}_i^2\rangle \end{pmatrix} \tag{12}$$

We now begin the calculations of the expectation values beginning with the idler mode:

$$E_i^2 = \hat{a}_i^2 + \hat{a}_i^{\dagger 2} + \hat{a}_i\hat{a}_i^\dagger + \hat{a}_i^\dagger\hat{a}_i. \tag{13}$$

Due to the orthogonality of the Fock state basis, we can determine that the matrix elements associated with the $\hat{a}_i^2$ and $\hat{a}_i^{\dagger 2}$ in the following sum:

$$\left\langle\psi|\hat{E}_i^2|\psi\right\rangle \tag{14}$$

$$= \gamma^2\sum_{n=0}^{\infty}\sum_{m=0}^{\infty}\beta^{n+m}\left\langle m,m|\hat{a}_i^2 + \hat{a}_i^{\dagger 2} + \hat{a}_i\hat{a}_i^\dagger + \hat{a}_i^\dagger\hat{a}_i|n,n\right\rangle \tag{15}$$

to be zero, leaving only the cross terms.

The first cross term can be found in the following manner:

$$\begin{aligned}\left\langle\psi|\hat{a}_i\hat{a}_i^\dagger|\psi\right\rangle &= \gamma^2\sum_{n=0}^{\infty}\sum_{m=0}^{\infty}\beta^{n+m}\left\langle m,m|\hat{a}_i\hat{a}_i^\dagger|n,n\right\rangle \\ &= \gamma^2\sum_n\left(\frac{N_s}{N_s+1}\right)^n n + \gamma^2\sum_n\left(\frac{N_s}{N_s+1}\right)^n\end{aligned} \tag{16}$$

To evaluate this, we use the identity:

$$\sum_n x^n n = \frac{x}{(1-x)^2} \tag{17}$$

To find:

$$\begin{aligned}\gamma^2\sum_n\left(\frac{N_s}{N_s+1}\right)^n n &= \frac{1}{N_s+1}\frac{\frac{N_s}{N_s+1}}{\left(1-\frac{N_s}{N_s+1}\right)^2} \\ &= N_s\end{aligned} \tag{18}$$

and:

$$\frac{1}{N_s+1}\sum_n\left(\frac{N_s}{N_s+1}\right)^n = 1 \tag{19}$$

where we have used the standard geometric series summation formula in Equation (19). Thus for $\langle \hat{a}_i \hat{a}_i^\dagger \rangle$ we obtain $N_s + 1$.

Following similar steps, the second cross term is found to be: $\langle \psi | \hat{a}_i^\dagger \hat{a}_i | \psi \rangle = N_s$. Combining all terms, we obtain:

$$\left\langle E_i^2 \right\rangle = 2N_s + 1 \tag{20}$$

For the correlation terms in the returned signal path, we have to additionally calculate the contribution of the noise added by the free space channel. This is done by defining $\hat{a}_R$, where $\hat{a}_R$ equals [26]:

$$\hat{a}_R = \sqrt{\kappa}\hat{a}_s + \sqrt{1-\kappa}\hat{a}_B \tag{21}$$

where κ is the transmissivity in the signal path, and $\hat{a}_B$ is the thermal noise mode. We then use this to calculate the electric field in the returned mode, $\langle E_R^2 \rangle$. These modes contain a mean photon number of $\frac{N_B}{1-\kappa}$.

$$\hat{E}_R = \hat{a}_R + \hat{a}_R^\dagger = \sqrt{\kappa}\left(\hat{a}_s + \hat{a}_s^\dagger\right) + \sqrt{1-\kappa}\left(\hat{a}_B + \hat{a}_B^\dagger\right)$$

Following a similar procedure to E_i^2, we find that the non-zero terms of E_R^2 are:

$$\hat{E}_R^2 = \kappa\left[\hat{a}_s\hat{a}_s^\dagger + \hat{a}_s^\dagger\hat{a}_s\right] + (1-\kappa)\left[\hat{a}_B\hat{a}_B^\dagger + \hat{a}_B^\dagger\hat{a}_B\right]. \tag{22}$$

where the expectation value is evaluated, and it is found to be:

$$\left\langle \hat{E}_R^2 \right\rangle = 2\kappa N_s + 2N_B + 1 \tag{23}$$

We note that if there exists no noise in the channel, i.e., $N_B = 0$, and perfect transmission, i.e., $\kappa = 1$, then Equation (23) reduces to Equation (20). Next, we calculate the covariance terms, which are of more importance for radar purposes as they quantify the correlation between the returned and idler photons. More explicitly, we calculate $\langle E_R E_i \rangle$ where: $E_R E_i = \hat{a}_R\hat{a}_i + \hat{a}_R^\dagger\hat{a}_i^\dagger + \hat{a}_R\hat{a}_i^\dagger + \hat{a}_R^\dagger\hat{a}_i$. In a similar manner to previous calculations, we begin by using the orthogonality Fock States to recognize that $\langle a_R a_i^\dagger \rangle$ and $\langle a_R^\dagger a_i \rangle$ are equal to 0. Using similar steps as previous calculations it is determined the cross-correlation term is $\langle \hat{E}_R \hat{E}_i \rangle = 2\sqrt{\kappa N_s(N_s+1)}$, which finally yields the full covariance matrix for the electric field:

$$\begin{pmatrix} 2\kappa N_s + 2N_B + 1 & 2\sqrt{\kappa N_s(N_s+1)} \\ 2\sqrt{\kappa N_s(N_s+1)} & 2N_s + 1 \end{pmatrix} \tag{24}$$

Note how the covariance terms shown here are identical (up to a factor of 2) to those of the OPA implementation [26]. Recall that in our case, these off-diagonal terms arise from taking two separate electric field measurements, and correlating the stored data. This is significant because it provides mathematical justification that using a delay line and performing a joint measurement of the signal and idler modes is identical to immediately detecting the idler mode and correlating with later receiver signal modes. This validates the procedures of recent experiments [12, 16].

This result is due entirely to the fact that entanglement is destroyed, and a joint measurement no longer is useful in obtaining a quantum benefit. This does not however mean that the OPA method should be abandoned. Using this analog method to correlate is useful since it is difficult to measure low power photon events of a realistic noisy signal.

3. NUMBER OPERATOR COVARIANCE

The number operator refers to photon counting experiments. This can be used in a quantum radar system by immediately counting the photons of the idler beam and using post processing to correlate this binary waveform with the signal beam after it has returned [3, 27].

We begin this calculation by defining the number operator:

$$\hat{N} = \hat{a}^\dagger\hat{a} \tag{25}$$

Similarly to the electric field derivation, we use the two-mode squeezed state that is defined in Equation (4).

Much like the electric field operator, the number operator is also commutative:

$$[\hat{N}_1, \hat{N}_2] = \hat{N}_1\hat{N}_2 - \hat{N}_2\hat{N}_1 = 0 \tag{26}$$

which allows $\langle \hat{N}_1\hat{N}_2\rangle = \langle \hat{N}_2\hat{N}_1\rangle$. Due to this and the number operator producing a non-zero mean, the covariance matrix for the number operator is given by:

$$V = \begin{pmatrix} \langle \hat{N}_s^2\rangle - \langle \hat{N}_s\rangle\langle \hat{N}_s\rangle & \langle \hat{N}_R\hat{N}_i\rangle - \langle \hat{N}_R\rangle\langle \hat{N}_i\rangle \\ \langle \hat{N}_i\hat{N}_R\rangle - \langle \hat{N}_i\rangle\langle \hat{N}_R\rangle & \langle \hat{N}_i^2\rangle - \langle \hat{N}_i\rangle\langle \hat{N}_i\rangle \end{pmatrix} \tag{27}$$

Now we begin the calculations for the expectation value of the idler mode:

$$\langle \hat{N}_i^2\rangle - \langle \hat{N}_i\rangle\langle \hat{N}_i\rangle \tag{28}$$

where we first define:

$$\hat{N}_i^2 = \hat{a}_i^\dagger\hat{a}_i\hat{a}_i^\dagger\hat{a}_i \tag{29}$$

This term can be seen to be non-zero due to the orthogonality of the Fock State basis, therefore it can be applied to the two-mode squeezed vacuum state:

$$\begin{aligned} \left\langle \psi|\hat{N}_i^2|\psi\right\rangle &= \gamma^2 \sum_{n=0}^{\infty}\sum_{m=0}^{\infty} \beta^{n+m} \left\langle m,m|\hat{a}_i^\dagger\hat{a}_i\hat{a}_i^\dagger\hat{a}_i|n,n\right\rangle \\ &= \gamma^2 \sum_n \left(\frac{N_s}{N_s+1}\right)^n n^2 \end{aligned} \tag{30}$$

Using the identity $\sum_{n=0}^{\infty} x^n n^2 = -\frac{x(1+x)}{(x-1)^3}$, we obtain:

$$\left\langle \hat{N}_i^2\right\rangle = -\gamma^2\frac{\beta(1+\beta)}{(\beta-1)^3} = N_s(1+2N_s) \tag{31}$$

It can also be seen that $\hat{N}_i = \hat{a}_i^\dagger\hat{a}_i$, where the expectation value was already calculated in the previous section to be N_s, therefore:

$$\langle \hat{N}_i^2\rangle - \langle \hat{N}_i\rangle\langle \hat{N}_i\rangle = N_s(1+N_s) \tag{32}$$

Next, the signal variance is evaluated and determined to be:

$$\langle \hat{N}_R^2\rangle - \langle \hat{N}_R\rangle\langle \hat{N}_R\rangle = \kappa^2 N_s(1+N_s) + N_B(1-\kappa+N_B) \tag{33}$$

and the cross-correlation terms expectation values are found to be:

$$\langle \hat{N}_s\hat{N}_i\rangle - \langle \hat{N}_s\rangle\langle \hat{N}_i\rangle = \kappa N_s(1+N_s) \tag{34}$$

This gives the full covariance matrix for the number operator:

$$V = \begin{pmatrix} \kappa^2 N_s(1+N_s) + N_B(1-\kappa+N_B) & \kappa N_s(1+N_s) \\ \kappa N_s(1+N_s) & N_s(1+N_s) \end{pmatrix} \tag{35}$$

It is again seen that when the transmissivity is perfect ($\kappa = 1$) and the system is noiseless ($N_B = 0$), then the on-diagonal terms are equal.

Finally, it should be noted that the cross correlation term for the number operator matches the covariance of the electric field operator, except that they are squared due to the quadratic nature in the field mode of the number operator while the electric field operator is linear.

In regards to comparing to other systems, it can be problematic to directly compare covariances. It is more appropriate to normalize the covariance to produce the correlation coefficients. This is done by simply dividing each covariance term by the product of the variances. This will be done in Section 5.

4. ELECTRIC FIELD QUADRATURE COVARIANCE

As a method to give a more direct comparison to some of the other research that has been conducted in the field [16, 18], we also discuss the electric field quadrature measurements. To do this, we first define the covariance matrix:

$$V = \begin{pmatrix} \{\hat{I}_i, \hat{I}_i\} & \{\hat{I}_i, \hat{Q}_i\} & \{\hat{I}_i, \hat{I}_R\} & \{\hat{I}_i, \hat{Q}_R\} \\ \{\hat{Q}_i, \hat{I}_i\} & \{\hat{Q}_i, \hat{Q}_i\} & \{\hat{Q}_i, \hat{I}_R\} & \{\hat{Q}_i, \hat{Q}_R\} \\ \{\hat{I}_R, \hat{I}_i\} & \{\hat{I}_R, \hat{Q}_i\} & \{\hat{I}_R, \hat{I}_R\} & \{\hat{I}_R, \hat{Q}_R\} \\ \{\hat{Q}_R, \hat{I}_i\} & \{\hat{Q}_R, \hat{Q}_i\} & \{\hat{Q}_R, \hat{I}_R\} & \{\hat{Q}_R, \hat{Q}_R\} \end{pmatrix} \tag{36}$$

where $\{\cdot, \cdot\}$ represents the anti-commutator, $I = \frac{1}{2}(\hat{a}^\dagger + \hat{a})$, and $Q = \frac{i}{2}(\hat{a}^\dagger - \hat{a})$ and the subscripts refer to the idler or return path.

As done in previous sections, non-zero terms are determined due to the orthogonality of the Fock state basis which is shown in Equation (37). It can be noted that all of these terms have been calculated in previous sections. The evaluated covariance matrix is shown in Equation (38). Note how the off-diagonal elements of the covariance matrix matches the off-diagonal elements of both of the previous covariance matrices up to a multiplicative constant. For the quadrature covariance, a 1/2 factor account for the fact the the correlations are split between I and Q.

$$V = \frac{1}{2}\begin{pmatrix} \frac{1}{4}(\hat{a}_i^\dagger\hat{a}_i + \hat{a}_i\hat{a}_i^\dagger) & \frac{i}{4}(\hat{a}_i\hat{a}_i^\dagger - \hat{a}_i^\dagger\hat{a}_i) & \frac{1}{4}(\hat{a}_i^\dagger\hat{a}_R^\dagger + \hat{a}_i\hat{a}_R) & \frac{i}{4}(\hat{a}_i^\dagger\hat{a}_R^\dagger - \hat{a}_i\hat{a}_R) \\ +\frac{1}{4}(\hat{a}_i\hat{a}_i^\dagger + \hat{a}_i^\dagger\hat{a}_i) & +\frac{i}{4}(\hat{a}_i^\dagger\hat{a}_i - \hat{a}_i\hat{a}_i^\dagger) & +\frac{1}{4}(\hat{a}_i^\dagger\hat{a}_R^\dagger + \hat{a}_i\hat{a}_R) & +\frac{i}{4}(\hat{a}_i^\dagger\hat{a}_R^\dagger - \hat{a}_i\hat{a}_R) \\ \frac{i}{4}(\hat{a}_i^\dagger\hat{a}_i - \hat{a}_i\hat{a}_i^\dagger) & \frac{1}{4}(\hat{a}_i^\dagger\hat{a}_i + \hat{a}_i\hat{a}_i^\dagger) & \frac{i}{4}(\hat{a}_i^\dagger\hat{a}_R^\dagger - \hat{a}_i\hat{a}_R) & -\frac{1}{4}(\hat{a}_i^\dagger\hat{a}_R^\dagger + \hat{a}_i\hat{a}_R) \\ +\frac{i}{4}(\hat{a}_i\hat{a}_i^\dagger - \hat{a}_i^\dagger\hat{a}_i) & +\frac{1}{4}(\hat{a}_i^\dagger\hat{a}_i + \hat{a}_i\hat{a}_i^\dagger) & +\frac{i}{4}(\hat{a}_i^\dagger\hat{a}_R^\dagger - \hat{a}_i\hat{a}_R) & +-\frac{1}{4}(\hat{a}_i^\dagger\hat{a}_R^\dagger + \hat{a}_i\hat{a}_R) \\ \frac{1}{4}(\hat{a}_i^\dagger\hat{a}_R^\dagger + \hat{a}_i\hat{a}_R) & \frac{i}{4}(\hat{a}_i^\dagger\hat{a}_R^\dagger + \hat{a}_i\hat{a}_R) & \frac{1}{4}(\hat{a}_R^\dagger\hat{a}_R + \hat{a}_R\hat{a}_R^\dagger) & \frac{i}{4}(\hat{a}_R\hat{a}_R^\dagger - \hat{a}_R^\dagger\hat{a}_R) \\ +\frac{1}{4}(\hat{a}_i^\dagger\hat{a}_i^\dagger + \hat{a}_i\hat{a}_R) & +\frac{i}{4}(\hat{a}_i^\dagger\hat{a}_R^\dagger - \hat{a}_i\hat{a}_R) & +\frac{1}{4}(\hat{a}_R^\dagger\hat{a}_R + \hat{a}_R\hat{a}_R^\dagger) & +\frac{i}{4}(\hat{a}_R^\dagger\hat{a}_R - \hat{a}_R\hat{a}_R^\dagger) \\ \frac{i}{4}(\hat{a}_i^\dagger\hat{a}_R^\dagger - \hat{a}_i\hat{a}_R) & -\frac{1}{4}(\hat{a}_i^\dagger\hat{a}_R^\dagger + \hat{a}_i\hat{a}_R) & \frac{i}{4}(\hat{a}_R^\dagger\hat{a}_R - \hat{a}_R\hat{a}_R^\dagger) & \frac{1}{4}(\hat{a}_R^\dagger\hat{a}_R + \hat{a}_R\hat{a}_R^\dagger) \\ +\frac{i}{4}(\hat{a}_i^\dagger\hat{a}_R^\dagger - \hat{a}_i\hat{a}_R) & -\frac{1}{4}(\hat{a}_i^\dagger\hat{a}_R^\dagger + \hat{a}_i\hat{a}_R) & +\frac{i}{4}(\hat{a}_R\hat{a}_R^\dagger - \hat{a}_R^\dagger\hat{a}_R) & \frac{1}{4}(\hat{a}_R^\dagger\hat{a}_R + \hat{a}_R\hat{a}_R^\dagger) \end{pmatrix} \tag{37}$$

$$V = \begin{pmatrix} \frac{1}{4}(2N_s + 1) & 0 & \frac{1}{2}\sqrt{\kappa N_s(N_s+1)} & 0 \\ 0 & \frac{1}{4}(2N_s + 1) & 0 & -\frac{1}{2}\sqrt{\kappa N_s(N_s+1)} \\ \frac{1}{2}\sqrt{\kappa N_s(N_s+1)} & 0 & \frac{1}{4}(2\kappa N_s + 2N_B + 1) & 0 \\ 0 & -\frac{1}{2}\sqrt{\kappa N_s(N_s+1)} & 0 & \frac{1}{4}(2\kappa N_s + 2N_B + 1) \end{pmatrix} \tag{38}$$

5. ANALYSIS

As mentioned earlier, there is no commutation between the electric field operator and the number operator, which means that if it is possible to determine the electric field with certainty, there is no information known about the photon count and vice versa. The claim of this paper is not a dual-measurement of the photon count and the electric field measurement, but to show the relationship between the covariance of these independent measurements in separate systems. To make the electric

field able to be compared directly with the number operator and quadrature, the correlation coefficient must be found for each. This correlation coefficient can be found using:

$$r_{xy} = \frac{\mathrm{cov}(x, y)}{\sqrt{\sigma_x \sigma_y}} \tag{39}$$

where σ represents the standard deviation. The necessary terms have already been calculated for all three measurement schemes. Therefore, for the electric field:

$$r_{E_{si}} = \frac{\left\langle \hat{E}_s \hat{E}_i \right\rangle}{\sqrt{\left\langle \hat{E}_s^2 \right\rangle \left\langle \hat{E}_i^2 \right\rangle}} = \frac{2\sqrt{\kappa N_s}}{\sqrt{2\kappa N_s + 2N_B + 1}} \tag{40}$$

It is easily found that the correlation coefficient for the quadrature method is identical to that of the electric field. Although this implies identical performance, in practice, multiple quadratures are being measured, and they can be combined in various ways to construct detector functions which yield differing performance [16, 18]. Therefore, one would expect better performance overall simply by the nature of collecting more information (multiple measurements). Here, we ignore these complexities and simply show them to be equal as any single correlation between two quadratures will result in identical performance.

For photon counting, the correlation coefficient is found to be:

$$r_{N_{si}} = \frac{\left\langle \hat{N}_s \hat{N}_i \right\rangle}{\sqrt{\left\langle \hat{N}_s^2 \right\rangle \left\langle \hat{N}_i^2 \right\rangle}} = \frac{\kappa\sqrt{N_s(N_s+1)}}{\sqrt{\kappa^2 N_s(1+N_s) + N_B(1-\kappa+N_B)}} \tag{41}$$

To compare these correlation coefficients, curves are generated for each one over a given range of N_s, κ, and the background noise photons per mode N_B. In addition, each of the three curves will have a small N_s and large N_s behavior that dictates its overall performance. Due to all of these variables, there exist many possible scenarios where one particular sensor out-performs the others in particular N_s regimes. We cannot possibly showcase all of these scenarios, so we restrict the presentation of results to the most important outcomes learned by our parametric sweeps and a small subset of plots which we believe best represents these lessons. An expanded analysis of these many scenarios will be done in future work. A summary of the most important results are given below.

1) For very low N_s, the electric field and quadrature measurements appear to always outperform photon counting.
2) Photon-counting appears to be dominant as long as there are enough photons returning to the radar. For low transmissivity (high noise), it performs the worst out of all of the methods.
3) If N_B is not too small, changing its value does not appear to affect the general behaviors of the curves, but rather, will simply change the N_s regimes with which these behaviors occur.

Quantum radar applications focus in the regime where $N_B \gg N_s$. For the following plots, we choose an N_B of 10 with the understanding that entangled photon powers are such that N_s is on the order of 1×10^{-3} [28]. Figure 2 shows the various correlation coefficients for a scenario in which $\kappa = 0.7$. Note how for very low N_s, the electric field amplitude and quadrature measurements outperforms the photon counting method. For larger values of N_s, the photon counting method becomes dominant. Again note that the E-field and E-field quadrature curves are identical. However, as mentioned earlier, in practice, using quadratures will improve the performance because there are simply more measurements taking place and one can combine I and Q in various ways to obtain differing performance [16, 18].

Next, observe Figure 3 for a second scenario, one with the transmissivity much lower. In this case, there are not enough photons making it back to the radar for low N_s and consequently photon counting is the worst performer at this signal power. This is because at low signal powers and high background noise, it is easier for the background noise to dominate the correlation with accidentals. As N_s increases, more photons make it back to the receiver and photon counting becomes dominant again.

Figure 4 shows a correlation over a range of N_s that is more typical of current SPDC power outputs to better illustrate the very low N_s regime performance. Clearly the electric field measurements perform better in this regime.

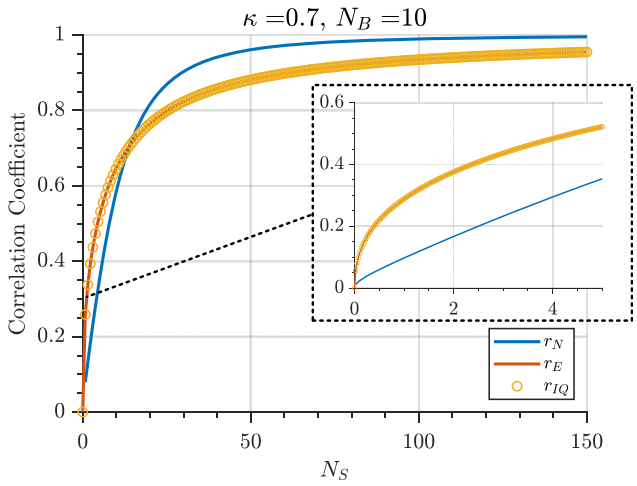

Figure 2. Correlation coefficient of the various methods for Scenario 1. ($\kappa = 0.7$, $N_B = 10$).

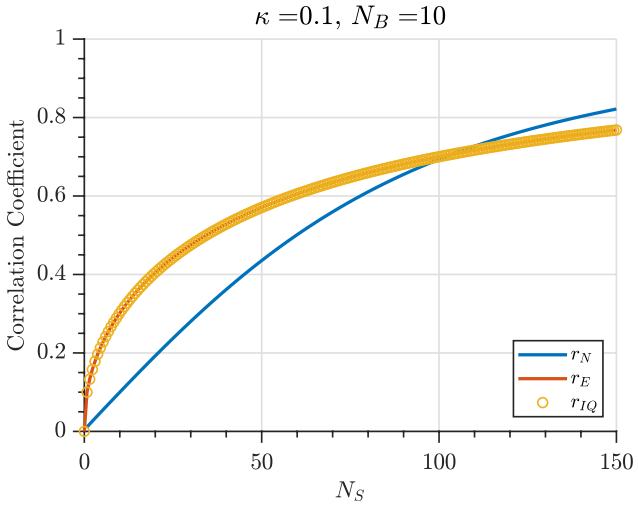

Figure 3. Correlation coefficient of the various methods for Scenario 2. ($\kappa = 0.1$, $N_B = 10$).

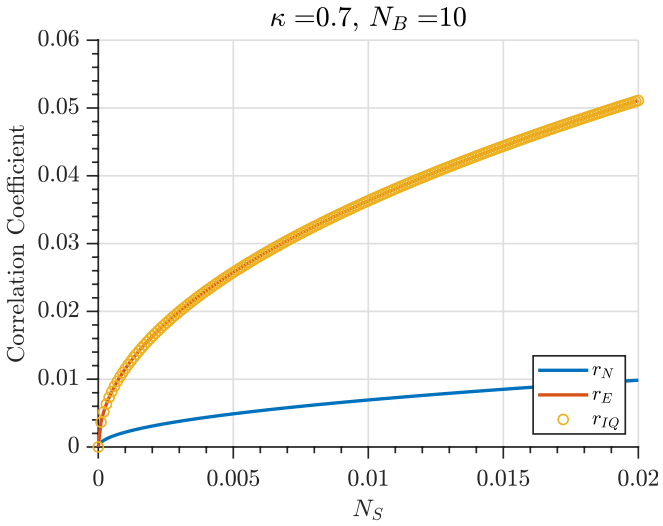

Figure 4. Correlation coefficient for low N_s for scenario 1.

6. CONCLUSION

In this paper, the correlation of the two-mode squeezed vacuum state has been evaluated, compared, and contrasted for three different quantum radar measurement strategies, all of which are post-correlation techniques (photon counting, E-field measurement, and quadrature measurement). It was found that the most optimal measurement strategy is a function of the transmit power N_s, background noise N_B, and transmissivity κ, depending on the regime of interest. Two particularly interesting scenarios were presented to showcase the behavior of the curves. One can experiment with the above equations for different scenarios of interest for trade-off analysis of the approaches presented herein. The work presented here can help to guide future experiments and applications in obtaining the most optimal design and implementation strategy.

ACKNOWLEDGMENT

This work is a collaborative effort between the Pennsylvania State Applied Research Laboratory and the Naval Engineering Education Consortium (NEEC) through NEEC Grant #N00174-19-1-0007 awarded by the Naval Surface Warfare Center, Crane Division.

REFERENCES

1. Luong, D., C. S. Chang, A. Vadiraj, A. Damini, C. Wilson, and B. Balaji, "Receiver operating characteristics for a prototype quantum two-mode squeezing radar," *IEEE Transactions on Aerospace and Electronic Systems*, Vol. 56, No. 3, 2041–2060, Jun. 2020.
2. Bowell, R. A., M. J. Brandsema, B. M. Ahmed, R. M. Narayanan, S. W. Howell, and J. M. Dilger, "Electric field correlations in quantum radar and the quantum advantage," *Proc. SPIE Conference on Radar Sensor Technology XXIV*, Vol. 11408, Apr. 2020, doi: 10.1117/12.2562749.
3. Brandsema, M. J., R. M. Narayanan, and M. Lanzagorta, "Correlation properties of single photon binary waveforms used in quantum radar/lidar," *Proc. SPIE Conference on Radar Sensor Technology XXIV*, Vol. 11408, Apr. 2020, doi: 10.1117/12.2560184.
4. Chang, C. W. S., A. M. Vadiraj, J. Bourassa, B. Balaji, and C. M. Wilson, "Quantum-enhanced noise radar," *Applied Physics Letters*, Vol. 114, No. 11, 112601, Mar. 2019.
5. Lanzagorta, M., *Quantum Radar*, Morgan & Claypool, San Rafael, CA, USA, 2011.
6. Lopaeva, E. D., I. Ruo Berchera, I. P. Degiovanni, S. Olivares, G. Brida, and M. Genovese, "Experimental realization of quantum illumination," *Physical Review Letters*, Vol. 110, No. 15, 153603, Apr. 2013.
7. Barzanjeh, S., S. Guha, C. Weedbrook, D. Vitali, J. H. Shapiro, and S. Pirandola, "Microwave quantum illumination," *Physical Review Letters*, Vol. 114, No. 8, 080503, Feb. 2015.
8. Shapiro, J. H., "The quantum illumination story," *IEEE Aerospace and Electronic Systems Magazine*, Vol. 35, No. 4, 8–20, Apr. 2020.
9. Bowell, R. A., M. J. Brandsema, R. M. Narayanan, S. W. Howell, and J. M. Dilger, "Tripartite correlation performance for use in quantum radar systems," *Proc. SPIE Conference on Radar Sensor Technology XV*, Vol. 11742, Apr. 2021, doi: 10.1117/12.2588308.
10. Lanzagorta, M., "Low-brightness quantum radar," *Proc. SPIE Conference on Radar Sensor Technology XIX and Active and Passive Signatures VI*, Vol. 9461, Baltimore, MD, Apr. 2015, doi: 10.1117/12.2177577.
11. Guha, S., "Receiver design to harness the quantum illumination advantage," *Proc. 2009 IEEE International Symposium on Information Theory (ISIT)*, Seoul, Korea, 963–967, Jun.–Jul. 2009.
12. Zhuang, Q. and J. H. Shapiro, "Ultimate accuracy limit of quantum pulse-compression ranging," arXiv:2109.11079v1, Sep. 2021.
13. Blakely, J. N., "Bounds on probability of detection error in quantum-enhanced noise radar," *Quantum Reports*, Vol. 2, No. 3, 400–413, Jul. 2020.
14. Tan, S.-H., B. I. Erkmen, V. Giovannetti, S. Guha, S. Lloyd, L. Maccone, S. Pirandola, and J. H. Shapiro, "Quantum illumination with Gaussian states," *Physical Review Letters*, Vol. 101, No. 25, 253601, Dec. 2008.
15. Dawood, M. and R. M. Narayanan, "Receiver operating characteristics for the coherent UWB random noise radar," *IEEE Transactions on Aerospace and Electronic Systems*, Vol. 37, No. 2, 586–594, Apr. 2001.
16. Luong, D., B. Balaji, and S. Rajan, "Biomedical sensing using quantum radars based on Josephson parametric amplifiers," *Proc. 2021 International Applied Computational Electromagnetics Society Symposium (ACES)*, Hamilton, ON, Aug. 2021, doi: 10.1109/ACES53325.2021.00091.
17. Russer, J. A., M. Würth, W. Utschick, F. Bischeltsrieder, and M. Peichl, "Performance considerations for quantum radar," *Proc. 2021 International Applied Computational Electromagnetics Society Symposium (ACES)*, Hamilton, ON, Aug. 2021, doi: 10.1109/ACES53325.2021.00105.

18. Luong, D., S. Rajan, and B. Balaji, "Quantum two-mode squeezing radar and noise radar: Correlation coefficients for target detection," *IEEE Sensors Journal*, Vol. 20, No. 10, 5221–5228, May 2020.
19. Liu, H., B. Balaji, and A. S. Helmy, "Target detection aided by quantum temporal correlations: Theoretical analysis and experimental validation," *IEEE Transactions on Aerospace and Electronic Systems*, Vol. 56, No. 5, 3529–3544, Oct. 2020.
20. Yang, H., W. Roga, J. D. Pritchard, and J. Jeffers, "Gaussian state-based quantum illumination with simple photodetection," *Optics Express*, Vol. 29, No. 6, 8199–8215, Mar. 2021.
21. England, D. G., B. Balaji, and B. J. Sussman, "Quantum-enhanced standoff detection using correlated photon pairs," *Physical Review A*, Vol. 99, 023828, Feb. 2019.
22. Scully, M. O. and M. S. Zubairy, *Quantum Optics*, Cambridge University Press, Cambridge, UK, 1997.
23. Vourdas, A., "Optical signals with thermal noise," *Physical Review A*, Vol. 39, No. 1, 206–213, Jan. 1989.
24. Helstrom, C. W., *Quantum Detection and Estimation Theory*, Academic Press, New York, NY, USA, 1976.
25. Griffiths, D. J. and D. F. Schroeter, *Introduction to Quantum Mechanics*, 3rd Edition, Cambridge University Press, Cambridge, UK, 2018.
26. Guha, S. and B. I. Erkmen, "Gaussian-state quantum illumination receivers for target detection," *Physical Review A*, Vol. 80, No. 5, 052310, Nov. 2009.
27. Ahmed, B. M., M. J. Brandsema, R. A. Bowell, R. M. Narayanan, S. W. Howell, and J. M. Dilger, "Remote sensing performance enhancement due to quantum+classical cooperative sensor," *Proc. SPIE Conference on Radar Sensor Technology XXIV*, Vol. 11408, Apr. 2020, doi: 10.1117/12.2562739.
28. Zhang, Z., S. Mouradian, F. N. Wong, and J. H. Shapiro, "Entanglement-enhanced sensing in a lossy and noisy environment," *Physical Review Letters*, Vol. 114, No. 11, 110506, Mar. 2015.